Supplementary Information for
Strong four-phonon interactions in α-GeTe

Yongheng Li[1], Bin Wei[1,8], Xinyue Zhang[3], Qi Ren[1], Chao Yang[1,9], Ziyan Gao[1], Xueyun Wang[1], Feihao Pan[4,5], Jinchen Wang[4,5], Kazuya Kamazawa[6], Mitsutaka Nakamura[7], Wei Luo[10,11], Yanzhong Pei[3*], Jiawang Hong[1,2*]

Affiliations

1. School of Aerospace Engineering, Beijing Institute of Technology, Beijing, 100081, China
2. Beijing Institute of Technology, Zhuhai Beijing Institute of Technology(BIT), Zhuhai 519088, China

3. Interdisciplinary Materials Research Center, School of Materials Science and Engineering, Tongji University, Shanghai, China

4. Beijing Key Laboratory of Optoelectronic Functional Materials and MicroNano

5. Devices, School of Physics, Renmin University of China, Beijing 100872, China

Key Laboratory of Quantum State Construction and Manipulation (Ministry of Education), Renmin University of China, Beijing, 100872, China

6. Neutron Science and Technology Center, Comprehensive Research Organisation for Science and Society (CROSS), Tokai, Ibaraki 319-1106, Japan

7. Materials and Life Science Division, J-PARC Center, Tokai, Ibaraki 319-1195, Japan

8. Henan Key Laboratory of Materials on Deep-Earth Engineering, School of Materials Science and Engineering, Henan Polytechnic University, Jiaozuo, China

9. College of physics and electronic information engineering, Guilin University of Technology, Guilin, 541008, China

10. Institute of High Energy Physics, Chinese Academy of Sciences (CAS), Beijing 100049, China

11. Spallation Neutron Source Science Center, Dongguan 523803, China

*corresponding author(s): yanzhong@tongji.edu.cn; hongjw@bit.edu.cn

Supplementary Note 1: Phonon self-energy and spectral function

The line shape including the four-phonon interaction are based the low-order perturbations. The phonon shift and phonon linewidth in phonon self-energy [Eq. (2)] can be described as below:[1,2]

$$
\begin{aligned}
\Delta^{(1)}_{\vec{q},s}(\Omega) &= \frac{24}{\hbar}\sum_{\vec{q}_1,s_1} V_4\left(\vec{q},s;-\vec{q},s;\vec{q}_1,s_1;-\vec{q}_1,s_1\right)\left(n_1+\frac{1}{2}\right) \\
&-\frac{18}{\hbar}\sum_{\vec{q}_1,s_1}\sum_{\vec{q}_2,s_2}\left|V_3\left(\vec{q},s;\vec{q}_1,s_1;\vec{q}_2,s_2\right)\right|^2 \\
&\times\mathcal{P}\left(\frac{n_1+n_2+1}{\omega+\omega_1+\omega_2}-\frac{n_1+n_2+1}{\omega-\omega_1-\omega_2}+\frac{n_1-n_2}{\omega-\omega_1+\omega_2}-\frac{n_1-n_2}{\omega+\omega_1+\omega_2}\right)
\end{aligned}
\tag{S1}
$$

$$
\begin{aligned}
\Gamma^{(1)}_{\vec{q},s}(\Omega) &= \frac{18\pi}{\hbar^2}\sum_{\vec{q}_1,s_1}\sum_{\vec{q}_2,s_2}\left|V_3\left(\vec{q},s;\vec{q}_1,s;\vec{q}_2,s\right)\right|^2 \\
&\times\Big\{\left(n_1+n_2+1\right)\left[\delta\left(\Omega-\omega_1-\omega_2\right)-\delta\left(\Omega+\omega_1+\omega_2\right)\right] \\
&+\left(n_1-n_2\right)\left[\delta\left(\Omega+\omega_1-\omega_2\right)-\delta\left(\Omega-\omega_1+\omega_2\right)\right]\Big\} \\
&+\Gamma_{\text{iso}}(\omega)
\end{aligned}
\tag{S2}
$$

$$
\begin{aligned}
\Delta^{(2)}_{\vec{q},s}(\Omega) &= -\frac{96}{\hbar^2}\sum_{\vec{q}_1,s_1}\sum_{\vec{q}_2,s_2}\sum_{\vec{q}_3,s_3}\left|V_4\left(\vec{q},s;\vec{q}_1,s_1;\vec{q}_2,s_2;\vec{q}_3,s_3\right)\right|^2 \\
&\times\mathcal{P}\Bigg\{\left[\left(n_1+1\right)\left(n_2+1\right)\left(n_3+1\right)-n_1n_2n_3\right]\times\left(\frac{1}{\Omega+\omega_1+\omega_2+\omega_3}-\frac{1}{\Omega-\omega_1-\omega_2-\omega_3}\right) \\
&+3\left[n_1\left(n_2+1\right)\left(n_3+1\right)-\left(n_1+1\right)n_2n_3\right]\times\left(\frac{1}{\Omega-\omega_1+\omega_2+\omega_3}-\frac{1}{\Omega+\omega_1-\omega_2-\omega_3}\right)\Bigg\} \\
&-\frac{576}{\hbar^2}\sum_{\vec{q}_1,s_1}\sum_{\vec{q}_1,s_2}\sum_{\vec{q}_3,s_3}V_4\left(\vec{q},s;-\vec{q},-s;-\vec{q}_1,s_1;\vec{q}_1,s_2\right)V_4\left(\vec{q}_1,s_1;-\vec{q}_1,s_2;\vec{q}_3,s_3;-\vec{q}_3,s_3\right) \\
&\times\mathcal{P}\left(\frac{n_1+n_2+1}{\omega_1+\omega_2}-\frac{n_1-n_2}{\omega_1-\omega_2}\right)\left(n_3+\frac{1}{2}\right)
\end{aligned}
\tag{S3}
$$

$$
\begin{aligned}
\Gamma^{(2)}_{\vec{q},s}(\Omega) &= \frac{96}{\hbar^2}\sum_{\vec{q}_1,s_1}\sum_{\vec{q}_2,s_2}\sum_{\vec{q}_3,s_3}\left|V_4\left(\vec{q},s;\vec{q}_1,s_1;\vec{q}_2,s_2;\vec{q}_3,s_3\right)\right|^2 \\
&\times\Big\{\left[\left(n_1+1\right)\left(n_2+1\right)\left(n_3+1\right)-n_1n_2n_3\right]\times\left[\delta\left(\Omega-\omega_1-\omega_2-\omega_3\right)-\delta\left(\Omega+\omega_1+\omega_2+\omega_3\right)\right]\Big\} \\
&+3\left[n_1\left(n_2+1\right)\left(n_3+1\right)-\left(n_1+1\right)n_2n_3\right]\times\left[\delta\left(\Omega+\omega_1-\omega_2-\omega_3\right)-\delta\left(\Omega-\omega_1+\omega_2+\omega_3\right)\right]\Big\}
\end{aligned}
\tag{S4}
$$

where V_3 and V_4 indicate scattering matrix related to cubic and quartic force constant, respectively.[3] Isotope scattering are taken in consideration as Γ_{iso}. δ- and $\mathcal{P}$ in Eq. S1-S4 are Dirac δ-function and the principal value, respectively. In numeral calculation, Gaussian function is applied to describe the Dirac δ-function and Kramers-Kronig (Hilbert) transformation to acquire $\Delta_{\vec{q},s}(\Omega)$. The n_i in Eq. S1-S4 are Bose distribution of the sth band at $\vec{q}$ phonon.

Considering the expensive computational resource required by four-phonon interactions, the spectral function and self-energy were calculated with coarse Monkhorst-Pack mesh-grid of 6×6×6. The obvious difference of the calculated total spectral function $S_{\vec{q},s}(\Omega)$ between considering $\Sigma^{(2)}_{\vec{q},s}(\Omega)$ and without considering can be found in Fig. 1 and Fig.S4-S5. In addition, Fig. 1 and Fig.S4-S5 illustrate that when considering $\Sigma^{(2)}_{\vec{q},s}(\Omega)$, which includes four-phonon scattering, the simulated imaginary dynamical susceptibility χ'' intensity become more consistent with experiment results. Figs. S6-S7 indicate the strong four-phonon interaction in boundary TA and TO branches, where without considering $\Sigma^{(2)}_{\vec{q},s}(\Omega)$ cannot well describe the temperature dependent linewidth extracted from INS experiment.

Supplementary Note 2: Temperature dependent phonon dispersion from inelastic neutron scattering experiment

We extracted temperature dependent phonon dispersion of α-GeTe in different Brillion zones (BZs) as shown in Figs. S1-S2. In different BZs, the χ'' ($\boldsymbol{Q}$, Ω) intensity of acoustic phonon bands will decrease obviously with increasing temperature. The boundary acoustic phonons unexpected harden as shown in Fig. S3a. However, the entire TO branch become obviously soft when temperature increase from 150K to 570K. As shown in Fig. S3b, the extracted phonon shift of TO at Q = (0, 1, 2.5) also indicate the boundary phonon soften about ~3meV. Besides, TO at center of BZ dramatically softening obviously in Figs. S1-S2, similar to water-fall phenomenon in PbTe. The tail of TO, as pointed by rows, are also very arresting in different BZs, especially at high temperature. It may be related to strong phonon-phonon scattering as described in main text.

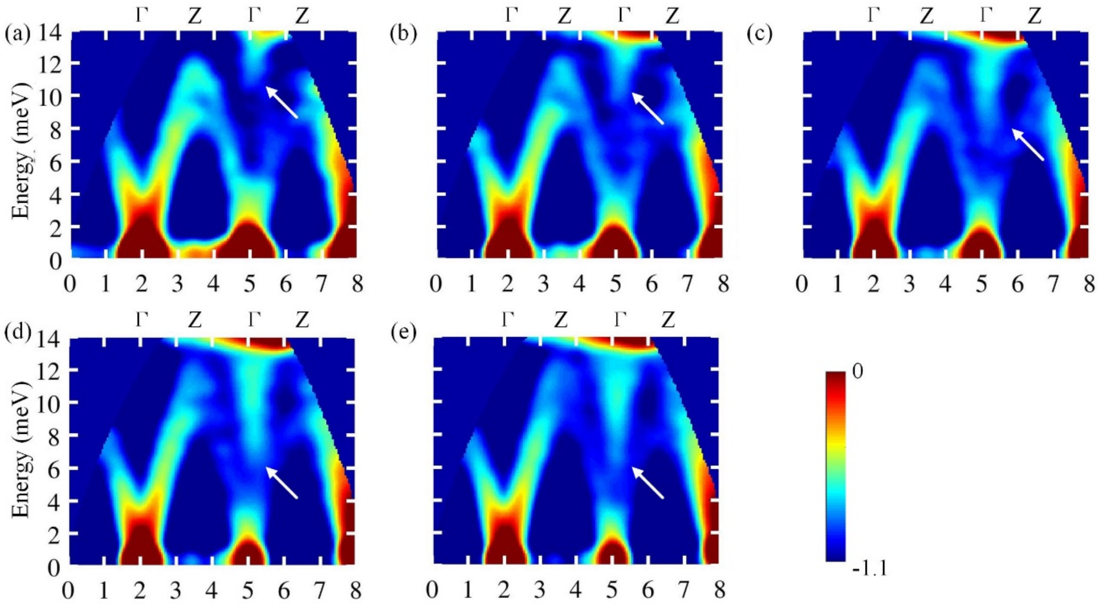

Figure S1 Temperature evolution of phonon dispersion $\chi''(\boldsymbol{Q}, \Omega)$ along [0-1L] direction on α-GeTe. Temperatures are 150K (a), 300K(b), 450K(c), 525K(d) and 570K(e). Intensities are integrated over $\pm$ 0.05 r.l.u. and plotted with $\log_{10}$ scale.

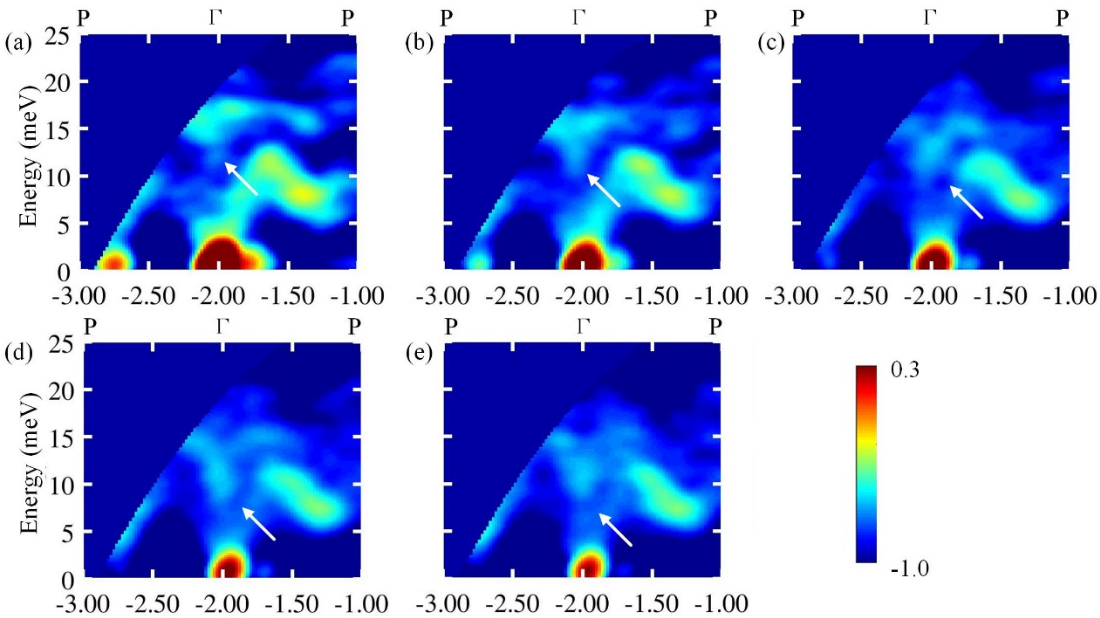

Figure S2 Temperature evolution of phonon dispersion $\chi''(\boldsymbol{Q}, \Omega)$ along [0K7] direction on α-GeTe. Temperatures are 150K (a), 300K(b), 450K(c), 525K(d) and 570K(e). Intensities are integrated over $\pm$ 0.1 r.l.u. and plotted with $\log_{10}$ scale.

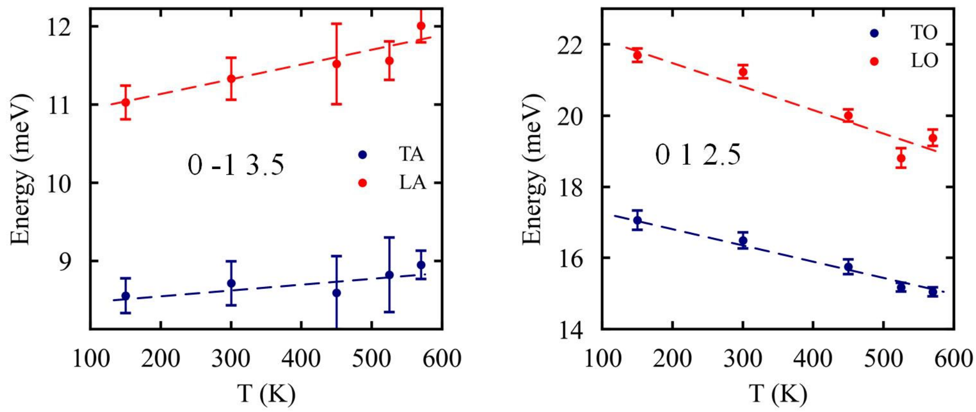

Figure S3 Temperature dependent boundary phonon shift at Q = (0, -1,3.5) and Q = (0, 1,2.5)

Supplementary Note 3: Important four-phonon scattering role at high temperature in predicting $\boldsymbol{\chi''_{\vec{q},j}(\Omega)}$

As shown in Figs. S4-S5, the four-phonon scattering plays important role in predicting better $\chi''_{\vec{q},j}(\Omega)$, especially at high temperature. In different BZs, we can find four-phonon scattering can effectively decrease the intensity of $\chi''_{\vec{q},j}(\Omega)$, especially at high temperature. This is related to the much larger $\Gamma^{(2)}_{\vec{k},s}(\Omega)$ at high temperature, which is in the denominator and quadratic as equation (1) shows. This observation aligns with the intuitive expectation of broader linewidths upon considering four-phonon interaction. Moreover, the quantitative analysis presented in this study confirms a significant increase in phonon linewidths when four-phonon scattering is included, supporting this explanation. At high temperatures, the TO and boundary TA modes exhibit noticeably broader linewidths, while their phonon energy shifts remain relatively unchanged, particularly for TA, when four-phonon scattering is accounted for in the calculation of $\chi''_{\vec{q},j}(\Omega)$.

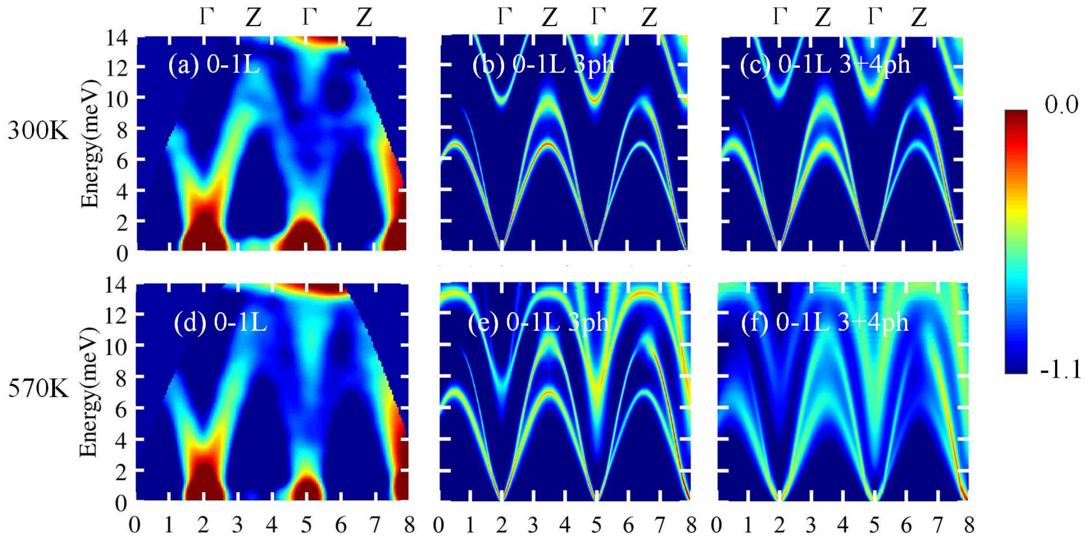

Figure S4 Phonon dispersions of α-GeTe at 150K (a-c) and 570K (d-f) along [0-1L] direction. The (a) and (d) are χ'' ($\boldsymbol{Q}$, Ω) measured with 4SEASONS using E_i=18 meV, which are integrated over ± 0.05 r.l.u. and plotted with $\log_{10}$ scale. (b) and (e) are calculated χ'' ($\boldsymbol{Q}$, Ω) with only three-phonon interaction while (c) and (f) are that with both three-phonon interaction and four-phonon interaction along [0-1L] direction.

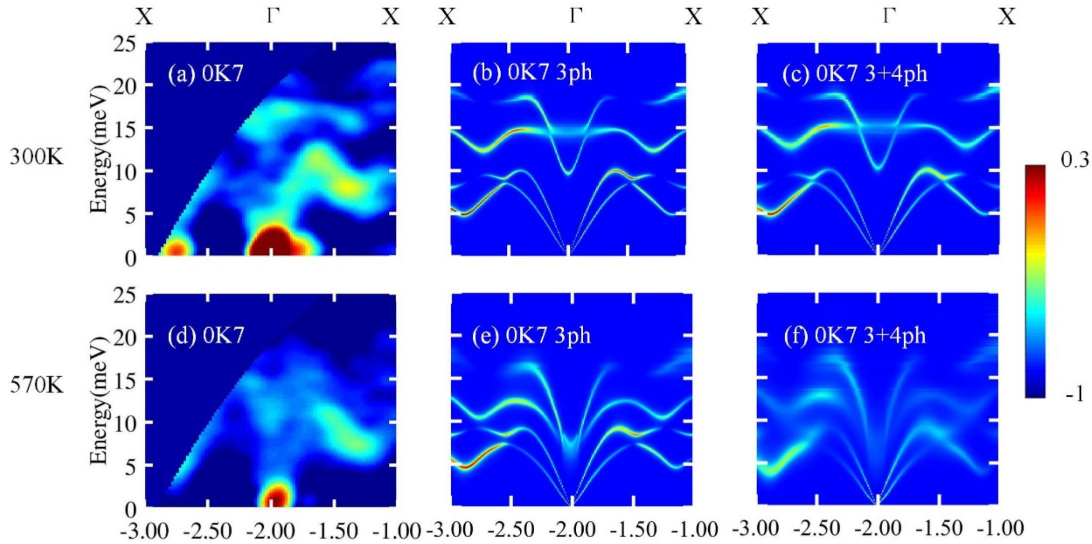

Figure S5 Phonon dispersions of α-GeTe at 150K (a-c) and 570K (d-f) along [0K7] direction. The (a) and (d) are χ'' ($\boldsymbol{Q}$, Ω) measured with 4SEASONS using E_i=30 meV, which are integrated over ± 0.1 r.l.u. and plotted with $\log_{10}$ scale. (b) and (e) are calculated χ'' ($\boldsymbol{Q}$, Ω) with only three-phonon interaction while (c) and (f) are that with both three-phonon interaction and four-phonon interaction along [0K7] direction.

Supplementary Note 4: Some typical extracted phonon shift and phonon linewidth

Figs. S6-S7 present the linewidths of TA and TO modes at high temperatures. The three-phonon interaction alone fails to accurately describe the energy broadening of boundary TA modes and several other TO modes beyond Q = (0, 1, 1.6). It indicates that the four-phonon interaction plays a significant role in the linewidths of TO and boundary TA modes. In contrast, for phonon shift, Fig. S8 shows that the four-phonon interaction has a minimal effect on phonon shifts, contributing only about ~0.5 meV at 570 K.

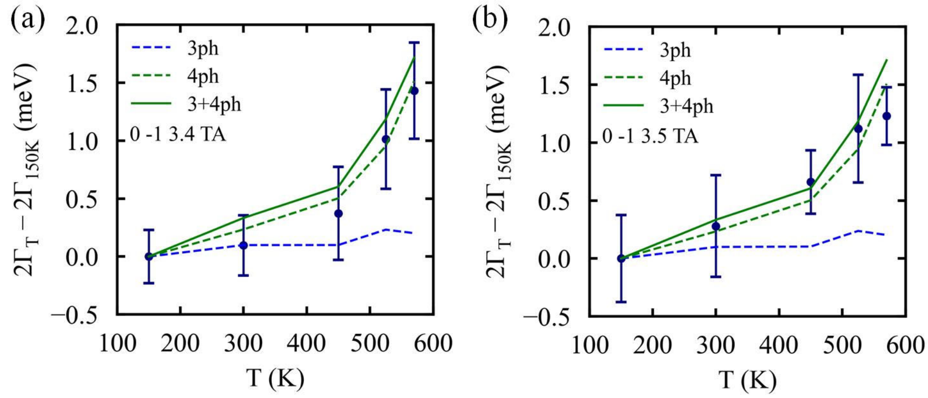

Figure S6 Energy broadenings of TA at Q = (0, -1, 3.4) and Q = (0, -1, 3.5) versus temperature. The blue dashed lines indicate contribution of three-phonon to energy broadenings while green dashed lines indicate contribution of four-phonon. The solid lines indicate contribution of both three- and four-phonon interaction to energy broadenings.

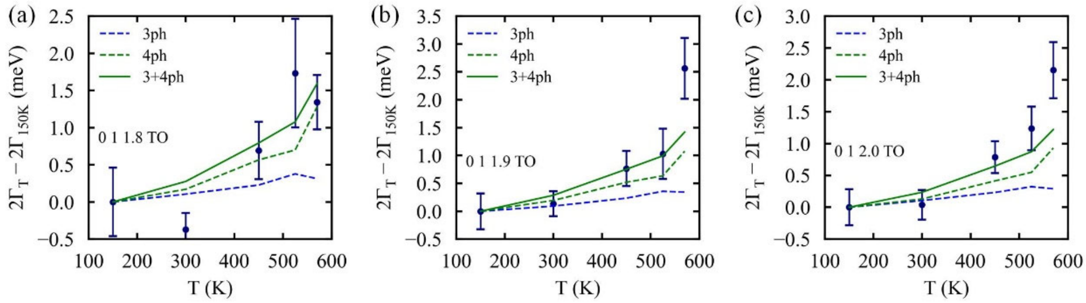

Figure S7 Energy broadenings of TO at Q = (0, 1, ξ) versus temperature, where ξ = 1.8, 1.9, 2.0. The blue dashed lines indicate contribution of three-phonon interaction to energy broadenings while green dashed lines indicate contribution of four-phonon interaction. The solid lines indicate contribution of both three- and four-phonon interaction to energy broadenings.

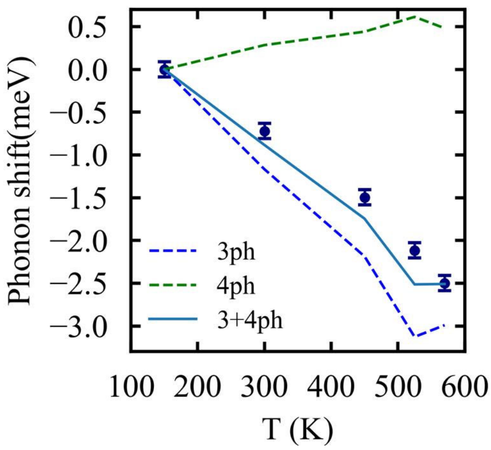

Figure S8 The phonon shift of TO at Q = (0, 1, 1.6) versus temperature. The blue dashed lines indicate contribution of three-phonon to phonon shift while green dashed lines indicate contribution of four-phonon. The solid lines indicate contribution of both three- and four-phonon interaction to phonon shift.

Supplementary Note 5: Temperature dependent calculation of lattice dynamic

We calculated temperature-dependent phonon dispersion as shown in Fig. S9a. The acoustic phonon modes at Z, especially LA mode, become harder when temperature increase from 150K to 570K. The optical mode softened obviously, especially for TO branch. Phonon density of state (Dos) in Fig. S9b is consistent to the change of phonon dispersion. When temperature increases up to 570K, there will be a clear shoulder at ~10meV, which reflects the harder LA and softer TO. Besides, the Dos peak around 15meV and 20meV at 150K will decrease to ~11meV and ~16meV respectively when temperature increase to 570K. The softened optical phonon will bring much more phonon-phonon interaction, including four-phonon scattering in α-GeTe.

Fig. S9c shows that the heat capacity almost keeps unchanged. Thus, it indicates the thermal conductivity is independent of changes in heat capacity. Fig. S9d indicates that there is little change of group velocity when temperature increases from 300K to 570K. Fig. S9e-f further confirm that the change of group velocity is small to lead to thermal conductivity of α-GeTe dramatically decrease at high temperature, even deviate from $\kappa_L \sim T^{-1}$ relation. So, scattering rate should be the main reason for the unusual temperature dependent thermal conductivity of α-GeTe.

We extracted the phonon dispersion along Γ-P and Γ-Z, which directions are closely related to κ_x and κ_z, and whole phonon Dos at 570 K, as shown in Fig. S10. There is phonon nesting between the boundary TA and TO branches along the Γ-Z direction, as indicated by the wide red lines in Fig. S10a. This phenomenon is associated with the tail of the TO mode at the zone center and is related to the strong four-phonon interaction described in the main text. As shown in Fig. S10c-d, when temperature increase from 300K to 570K, the four-phonon interaction phase space is comparable with three-phonon interaction phase space between ~6meV and ~14meV at 570K, as orange region shows. The orange region in Fig. S10d is consistent to the Fig. S10a-b. Thus, it confirms that phonon nesting is related to strong four-phonon interaction, as well as temperature effect. The temperature effect highlights two key points: (1) temperature-induced anharmonicity in α-GeTe and (2) a stronger temperature dependence of the four-phonon interaction compared to the three-phonon interaction.

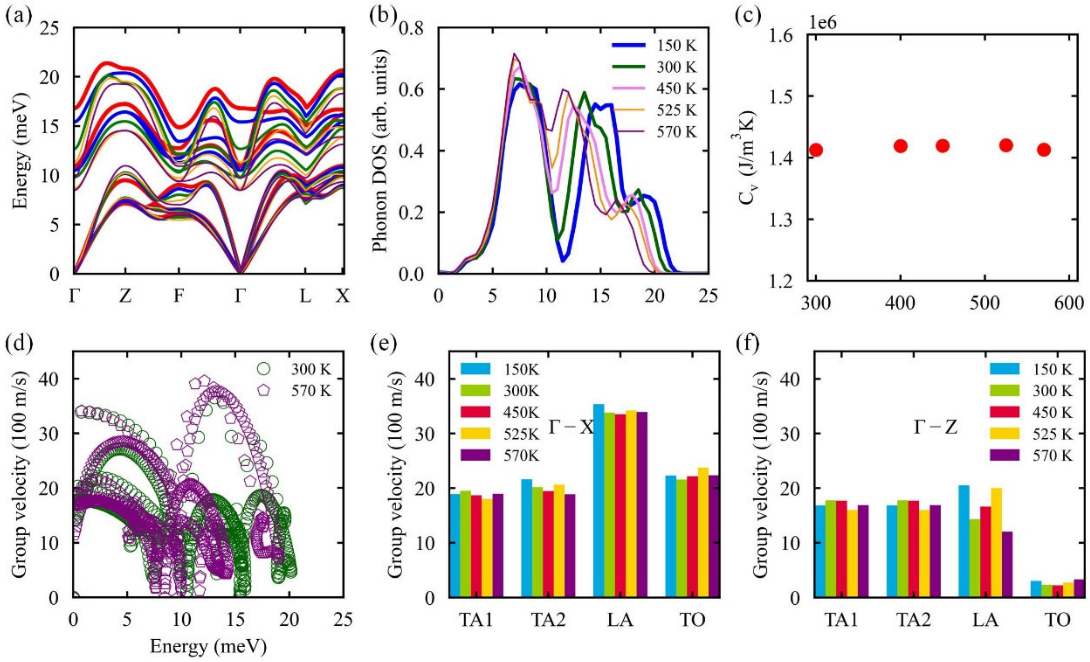

Figure S9 Temperature dependent phonon dispersion of α-GeTe (a) and temperature dependent phonon density of state (b). The same color of lines in (a) and (b) indicates the same temperature. (c) Temperature-dependence heat capacity, which is calculated with temperature dependent force constant. (d) Energy dependent group velocity at 300K and 570K. (e) and (f) are temperature dependent group velocity of TA_1, TA_2, LA and TO modes.

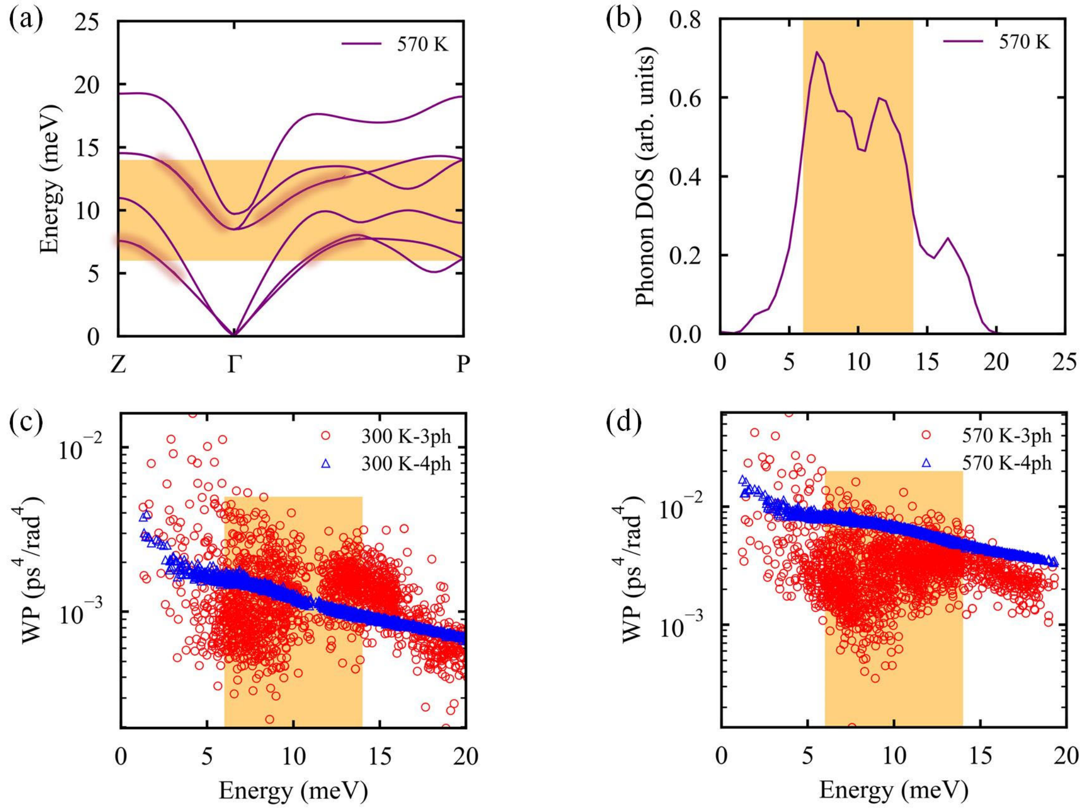

Figure S10 Phonon dispersion(a) and phonon density of state (b) of *α*-GeTe at 570K. wide red lines in (a) indicate phonon nesting. Weighted phase space versus phonon energy at 300K(e) and 570K(f). The orange regions in (a)-(d) indicate where the four-phonon interaction exhibits comparable strength with three-phonon interaction.

1. Klemens, P. G. Anharmonic Decay of Optical Phonons. *Phys. Rev.* **148**, 845–848 (1966).

2. Procacci, P., Cardini, G., Righini, R. & Califano, S. Anharmonic lattice dynamics and computer simulation for simple model systems. *Phys. Rev. B* **45**, 2113–2125 (1992).

3. Balkanski, M., Wallis, R. F. & Haro, E. Anharmonic effects in light scattering due to optical phonons in silicon. *Phys. Rev. B* **28**, 1928–1934 (1983).